

Oxygen transport at a ferroelastic domain wall in CaTiO<sub>3</sub>Robert Rauschen  and Roger A. De Souza \*

Institute of Physical Chemistry, RWTH Aachen University, 52056 Aachen, Germany



(Received 24 June 2022; accepted 9 November 2022; published 22 November 2022)

The formation and migration of charged oxygen vacancies at a 90°(100)[001] domain wall in orthorhombic CaTiO<sub>3</sub> were studied by means of atomistic simulation techniques. The segregation-energy profiles of an oxygen vacancy across the wall were revealed through careful discrimination to display hyperbolic secant forms, with a domain-wall width consistent with that obtained from a tilt-angle analysis. Equilibrium distributions of oxygen vacancies across the ferroelastic domain wall in a nominally undoped (weakly acceptor-doped) sample were calculated self-consistently (assuming a sech segregation-energy profile) for various temperatures. The calculations indicate a positively charged domain wall, arising from high vacancy concentrations, compensated by negative space-charge layers, in which vacancies are depleted. The activation barriers for oxygen-vacancy migration along the domain wall, determined from nudged-elastic-band calculations, revealed that the long-range diffusion of oxygen vacancies along the wall is neither strongly enhanced nor strongly hindered.

DOI: [10.1103/PhysRevMaterials.6.L111401](https://doi.org/10.1103/PhysRevMaterials.6.L111401)

The mineral perovskite (CaTiO<sub>3</sub>) adopts an orthorhombic ground-state structure, in which corner-sharing TiO<sub>6</sub> octahedra are tilted around all three pseudocubic axes [1,2]. The pattern of tilted octahedra is not uniform over an entire specimen of orthorhombic CaTiO<sub>3</sub>, but only within small regions, or domains. Between two domains, that is, at a domain wall, the three octahedral tilt angles change continuously from one orientation to the other over a nonzero length [3]. Domain walls in CaTiO<sub>3</sub> thus constitute regions of perturbed orthorhombic structure, and consequently, they are expected to display properties different from those of the parent lattice [4–6].

One such property is ion transport, which is believed to be faster along domain walls than in the parent perovskite lattice [3,7–10]. Faster oxygen diffusion along domain walls in CaTiO<sub>3</sub> was reported in an experimental study, with oxygen tracer diffusion coefficients  $D_{\text{O}}^{*\text{,dw}}/D_{\text{O}}^{*\text{,latt}} \approx 10^7$  [7]. Upon close examination, however, this result appears questionable. Since  $D_{\text{O}}^*$  is proportional to both the concentration of point defects responsible for transport (in this case, oxygen vacancies) and their diffusivity ( $D_{\text{O}}^* \propto c_{\text{v}} D_{\text{v}}$ ), the higher values of  $D_{\text{O}}^{*\text{,dw}}$  have to be due to higher  $c_{\text{v}}$ , higher  $D_{\text{v}}$ , or some combination thereof. An increase in  $D_{\text{v}}$  by orders of magnitude would presumably require a substantial decrease in the exponential term in  $D_{\text{v}} = D_{\text{v}}^0 \exp(-\Delta H_{\text{mig,v}}/k_{\text{B}}T)$ , rather than an unreasonably large increase in the preexponential term. The experimental result [7], however, is that the activation enthalpies are equal within experimental error,  $\Delta H_{D^*}^{\text{,dw}} \approx \Delta H_{D^*}^{\text{,latt}} (\approx 4 \text{ eV})$ . Consequently, the higher  $D_{\text{O}}^{*\text{,dw}}$  would appear to arise from an increase in  $c_{\text{v}}^{\text{,dw}}$ . On the one hand,  $c_{\text{v}}^{\text{,dw}} \gg c_{\text{v}}^{\text{,latt}}$  is expected—preferential formation of oxygen vacancies at domain walls in CaTiO<sub>3</sub> has been predicted [3,11]—but values of  $c_{\text{v}}^{\text{,dw}}$  have not

yet been calculated, and so it is unclear whether the lowered vacancy formation energy is quantitatively consistent with the measured increase. On the other hand, in order for  $c_{\text{v}}^{\text{,dw}}$  to have differed from  $c_{\text{v}}^{\text{,latt}}$  by  $10^7$ ,  $c_{\text{v}}^{\text{,latt}}$  would have to have been extraordinarily low, so that  $c_{\text{v}}^{\text{,dw}}$  did not exceed the density of available oxide-ion sites. A low  $c_{\text{v}}^{\text{,latt}}$ , in turn, would have required samples of exceptionally high purity. Undoped CaTiO<sub>3</sub> routinely contains several hundred ppm of oxygen vacancies that form to compensate acceptor-type defects [12–14]. Thus, the origin of the faster diffusion is unclear.

A further questionable issue is that the reported  $\Delta H_{D^*}^{\text{,latt}} = 4 \text{ eV}$  [7] is incredibly high, compared not only with values predicted from atomistic simulations for CaTiO<sub>3</sub> [15–17], but also with values measured for other titanate perovskites [18] (all <1 eV). In fact, it was suggested [17] that the measured diffusion profiles were misinterpreted. Given the doubts concerning the experimental study [7], the open question is, to what degree is oxygen diffusion along a domain wall in CaTiO<sub>3</sub> faster than in the regular lattice?

In this Letter, we used atomistic simulation techniques to answer this question, examining specifically the formation and migration of oxygen vacancies at the 90°(100)[001] domain wall in orthorhombic CaTiO<sub>3</sub> (space group *Pbnm*). Molecular static (MS) simulations were performed with the GULP code [19] and molecular dynamics (MD) simulations, with the LAMMPS code [20]. The empirical pair potentials (EPPs) derived by Pedone *et al.* [21] were used, because they have been shown in MD simulations to reproduce oxygen-vacancy transport kinetics in CaTiO<sub>3</sub> [17] extraordinarily well. Furthermore, they also correctly reproduce [17] CaTiO<sub>3</sub>'s phase transitions, *Pbnm* → *Cmcm* → *I4/mcm* → *Pm3m*, albeit with overestimated transition temperatures [1,2]. A simulation cell with two 90°(100)[001] domain walls was generated, in order to satisfy the requirements of periodic boundary conditions. The supercell contained 40×4×4 formula units of CaTiO<sub>3</sub> and had one domain wall at its center

\*desouza@pc.rwth-aachen.de

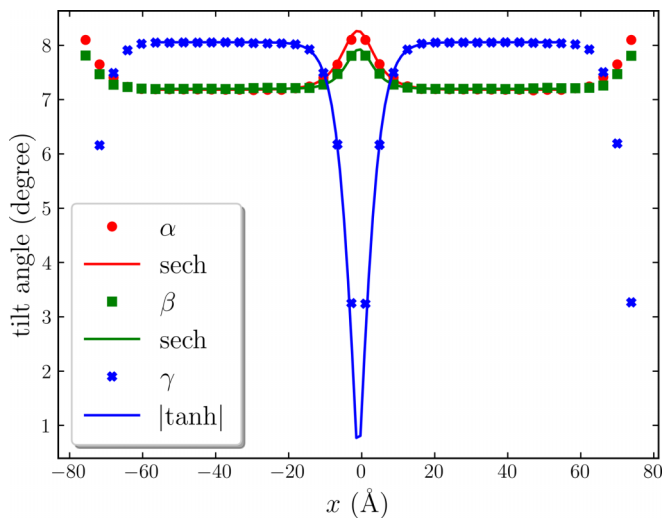


FIG. 1. Octahedral tilt angles around the three pseudocubic axes for a  $90^\circ(100)[001]$  domain wall in  $\text{CaTiO}_3$ . Symbols refer to data extracted from a relaxed supercell, with one wall at the center and one at the edge. Absolute values of the angles are shown for simplicity. Lines are the fits to Eqs. (1) and (2).

and one at its edge, the two separated by ca.  $70 \text{ \AA}$ , so that the interaction between the domain walls was negligible. The size and shape of the cell and the ion positions were then allowed to relax to a minimum-energy configuration in an MS simulation. We chose this domain wall, since it has already been examined computationally [3,11,22], and hence there are certain structural data with which we can compare our results.

The first comparison concerns the behavior of the tilt angles ( $\alpha$ ,  $\beta$ ,  $\gamma$ ) of the  $\text{TiO}_6$  octahedra around the three pseudocubic tilt axes. From the energy-minimized simulation cell, we extracted the tilt angles (with in-house software [23]). As seen in Fig. 1, the tilt angle around the  $[001]$  axis,  $\gamma$ , is diminished at the domain wall, following the form

$$\theta = \theta_0 \tanh\left(\frac{x - x_0}{w}\right); \quad (1)$$

it can thus be considered as a primary order parameter within Landau theory [3,11]. The tilt angles  $\alpha$  and  $\beta$  are enhanced at the wall, following

$$\theta = \theta_{\max} \operatorname{sech}\left(\frac{x - x_0}{w}\right) + \theta_0, \quad (2)$$

and can thus be considered as secondary order parameters. Fitting Eqs. (1) and (2) to the data of Fig. 1, we obtain a mean wall width of  $2w = (10.6 \pm 0.4) \text{ \AA}$ . This value is consistent with literature data for this wall, also obtained computationally, of  $10.9 \text{ \AA}$  [22],  $11.364 \text{ \AA}$  [3], and  $10.0 \text{ \AA}$  [24].

The second comparison concerns the excess energy of the domain wall. This quantity is obtained from the MS simulations as the difference in energies of cells with two walls and with zero walls, normalized to the cross-sectional area of the cell:  $\Delta_f E_{\text{dw}} = (E_{\text{cell}}^{2\text{dw}} - E_{\text{cell}}^{0\text{dw}})/(2A_{\text{cell}})$ . The value obtained, of  $\Delta_f E_{\text{dw}} = 135 \text{ mJ m}^{-2}$ , agrees well with the literature data of  $(160 \pm 10) \text{ mJ m}^{-2}$  [3] and  $116 \text{ mJ m}^{-2}$  [24]. In an analogous manner, the simulations yield the excess volume of the wall,  $\Delta_f V_{\text{dw}} = 0.0417 \text{ \AA}^3 \text{ \AA}^{-2}$ . Both  $\Delta_f E_{\text{dw}}$  and  $\Delta_f V_{\text{dw}}$  dis-

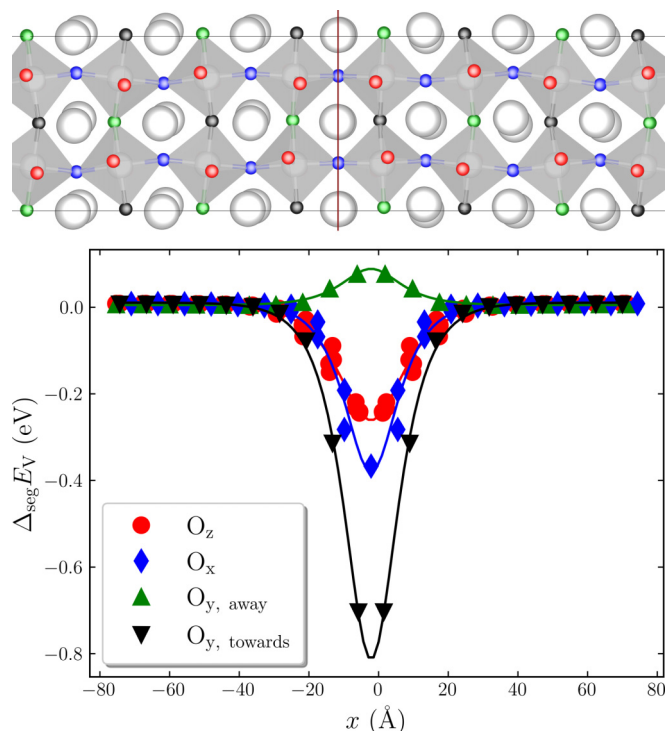


FIG. 2. Top: Structure of a  $90^\circ(100)[001]$  domain wall in orthorhombic  $\text{CaTiO}_3$ , as viewed along the  $z$  axis. The Ca ions are shown as isolated spheres, the Ti ions as spheres within the octahedra, and the O ions are color coded according to the direction in which they connect the  $\text{TiO}_6$  octahedra. Bottom: The segregation energy of an oxygen vacancy,  $\Delta_{\text{seg}} E_v$ , across the  $90^\circ(100)[001]$  wall. The color coding is the same as in the top part of the figure. The lines are fits to the appropriate versions of Eq. (2).

play rather low values compared with the equivalent data for low-angle grain boundaries in cubic  $\text{SrTiO}_3$  [25], indicating that the domain wall constitutes a relatively weak perturbation of the lattice.

Having established that these EPPs yield physically reasonable results for the wall's atomistic structure and formation energy, we now turn to the formation and migration of oxygen vacancies.

The oxygen-vacancy segregation energy  $\Delta_{\text{seg}} E_v$  is defined as the formation energy of an oxygen vacancy in the domain-wall cell relative to the value in the regular lattice:  $\Delta_{\text{seg}} E_v = \Delta_f E_v - \Delta_f E_v^{\text{latt}}$ . It is necessary, therefore, to differentiate between O1 and O2 positions in the  $\text{CaTiO}_3$  structure because the vacancy formation energy in the regular ( $Pbnm$ ) lattice differs slightly. The variation in  $\Delta_{\text{seg}} E_v$  across the cell was obtained through a series of Mott-Littleton calculations [19,26], in which an oxygen ion was removed from each site within the simulation cell (480 in total), and the system's energy was minimized. Although Mott-Littleton calculations are not strictly applicable to such cells, they have been applied successfully to examine oxygen-vacancy formation at low-angle tilt grain boundaries in  $\text{SrTiO}_3$  [25].

The results are shown in Fig. 2. With  $\Delta_{\text{seg}} E_v < 0$ , they indicate that most of the oxide-ion sites at the domain wall have a lower formation energy than in the bulk, confirming the results of earlier studies [3,11]. Our lowest value, of

$\Delta_{\text{seg}}E_v = -0.7$  eV, is comparable with literature data reported for this wall with other sets of pair potentials ( $-1.25$  eV [3];  $-0.58$  and  $-0.80$  eV [11]). Since  $\Delta_{\text{seg}}E_v < 0$  is also found for grain boundaries [27–31], surfaces [32–35], and dislocations [25,36–39] in titanate perovskites, we attribute  $\Delta_{\text{seg}}E_v < 0$  at the domain wall quite generally to the perturbation of the regular lattice structure at the extended defect. In Fig. 2, in addition to differentiating between O1 and O2 sites, we found that it was necessary to differentiate, within the domain wall, between three different types of O2 sites. (In this representation, it is helpful to consider that O1 ions connect  $\text{TiO}_6$  octahedra in the  $z$  direction, whereas the O2 ions connect the octahedra in  $x$  and  $y$  directions.) The lower symmetry induced by the domain wall splits the O2 ions into those that connect octahedra in the  $x$  direction (blue spheres in Fig. 1); those that connect octahedra in the  $y$  direction and are tilted towards the wall (black spheres); and those that connect octahedra in the  $y$  direction and are tilted away from the wall (green spheres). Only the last type is disfavored for vacancy formation. This detailed discrimination between oxygen sites revealed a new result: that the form of  $\Delta_{\text{seg}}E_v(x)$  across the wall adopts a hyperbolic secant form for all four domain-wall oxygen sites. Indeed, fitting Eq. (2) to the data yields  $2w = (10.44 \pm 0.14)$  Å, in good agreement with  $2w = (10.6 \pm 0.4)$  Å obtained above from the analysis of the tilt angles. Thus, not only crystal-structure parameters (tilt angles  $\alpha$  and  $\beta$ ) but also defect-structure parameters (defect formation energies) can be interpreted as secondary order parameters.

In order to obtain  $c_v^{\text{dw}}$  from  $\Delta_{\text{seg}}E_v < 0$ , we have to first specify  $c_v^{\text{latt}}$ , since equilibrium concentrations in the wall are relative to those in the regular lattice. Experimental studies of nominally undoped  $\text{CaTiO}_3$  [12–14] indicate that such samples are effectively acceptor doped, in line with studies of nominally undoped  $\text{SrTiO}_3$  [33,40–42] and  $\text{BaTiO}_3$  [43–45]. As long as the sample is not strongly reduced, the effective concentration of these acceptor species fixes the concentration of oxygen vacancies in the regular lattice,  $c_a^{\text{latt}} = 2c_v^{\text{latt}}$ . We took  $c_a^{\text{latt}} = 2 \times 10^{18} \text{ cm}^{-3}$  on the basis that  $c_a^{\text{latt}}$  should be neither too high (at the level of purposely added dopants) nor too low (at the level of exceptionally pure samples with exceptionally low intrinsic defect concentrations [46]). (Incidentally, there are three possible sources of acceptor-type cation species: lower-valent impurities, cation vacancies, and Ca antisites.)

Equilibrium values of  $c_v^{\text{dw}}$  were found by minimizing the Gibbs energy of a system containing a domain wall and mobile oxygen vacancies. Such an analytical treatment yields [28]

$$c_v(x) = \frac{N_v c_v^{\text{latt}} \exp\left[-\frac{\Delta_{\text{seg}}G_v(x) + 2e\phi(x)}{k_B T}\right]}{N_v - c_v^{\text{latt}} - c_v^{\text{latt}} \exp\left[-\frac{\Delta_{\text{seg}}G_v(x) + 2e\phi(x)}{k_B T}\right]}, \quad (3)$$

where  $\Delta_{\text{seg}}G_v(x)$  is the Gibbs segregation energy of an oxygen vacancy,  $N_v$  the volumetric density of oxide-ion lattice sites,  $e$  the elementary charge, and  $\phi(x)$  the electric potential, which was set arbitrarily to zero in the lattice. Note: A calculation based on a simple exponential term,  $c_v^{\text{dw}} \propto \exp(-\Delta_{\text{f}}E_v/k_B T)$ , cannot be applied here because it fails to include electrochemical equilibrium between oxygen vacan-

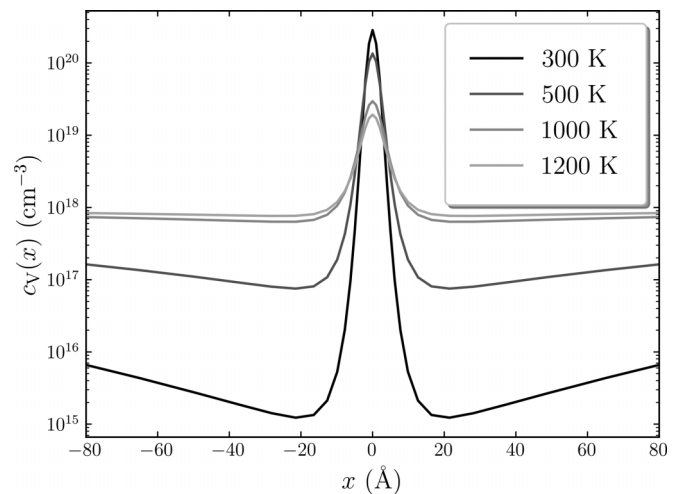


FIG. 3. Equilibrium oxygen-vacancy concentrations at and around a domain wall in weakly acceptor-doped  $\text{CaTiO}_3$  ( $c_a^{\text{latt}}/2 = c_v^{\text{latt}} = 10^{18} \text{ cm}^{-3}$ ) at four different temperatures. Profiles calculated self-consistently from the segregation-energy profiles shown in Fig. 2.

cies in the domain wall and those in the regular lattice, and because it ignores that oxygen vacancies are charged.

The standard approach in the literature is to approximate  $\Delta_{\text{seg}}G_v(x)$  with a rectangular function at the interface, the so-called abrupt core|space-charge model [47]. In view of the results of Fig. 2, a superior (and more natural) approach is to use a continuous sech form for  $\Delta_{\text{seg}}G_v(x)$ . Assuming the segregation entropy and the pressure-volume term to be negligible, we set  $\Delta_{\text{seg}}G_v(x) \approx \Delta_{\text{seg}}E_v(x)$ .

In order to obtain self-consistent values for  $c_v(x)$  and  $\phi(x)$ , the Poisson equation {with  $\epsilon_0\epsilon_r$  as the dielectric permittivity, and  $\epsilon_r(T)$  taken from the literature [48,49]},

$$\epsilon_0\epsilon_r \frac{d^2\phi}{dx^2} = ec_a^{\text{latt}} - 2ec_v(x), \quad (4)$$

has to be solved for the entire domain, with  $c_v(x)$  given by Eq. (3). As boundary conditions, the electric potential and field are taken to be zero in the lattice, far away from the domain wall. By writing Eq. (4) in this form, we have assumed (i) that the acceptor cation species are immobile, and hence, their concentration is constant (this is true for cations in perovskites at all but the highest temperatures [50]); and (ii) that the concentrations of electronic species are negligible compared with  $c_a^{\text{latt}}$ , which is true for all but highly reducing conditions [13,14]. Numerical solutions were obtained by finite-element-method calculations, and the results are shown in Fig. 3 for four selected temperatures.

The domain wall is indeed predicted quantitatively to have a higher equilibrium oxygen-vacancy concentration than the regular lattice. At  $T = 300$  K,  $c_v^{\text{dw}}(x)$  peaks at over 250 times  $c_v^{\text{latt}}$  ( $=10^{18} \text{ cm}^{-3}$ ), but the more relevant quantity for transport,  $\langle c_v^{\text{dw}} \rangle$ , the average value over the width of the wall, is only a factor of 67 higher. At the two highest temperatures considered in Fig. 3, the degree of enhancement decreases to  $\langle c_v^{\text{dw}} \rangle / c_v^{\text{latt}} \approx 10$ . The positive charge of the segregated oxygen vacancies is compensated by two negatively charged, diffuse space-charge zones in which oxygen vacancies are depleted.

These zones extend up to hundreds of angstroms on each side of the wall (not shown); with increasing temperature, the degree of vacancy redistribution to the wall is less pronounced, and the extension is much smaller as well.

Three points are worth emphasizing. First,  $c_v$  is modified at and in the vicinity of the domain wall, not because of any intrinsic wall charge (as in head-to-head and tail-to-tail ferroelectric domain walls [51,52]) or because of the effects of surfaces [53], but because of a thermodynamic driving energy,  $\Delta_{\text{seg}}E_v < 0$ . Second, the positive charge of the wall means that electrons, as mobile negatively charged defects, will be accumulated within the space-charge zones and within the domain wall, generating enhanced electron conduction, certainly within the space-charge zones, and possibly within the wall (as long as the electron mobility along the wall is not diminished substantially). Third, other ferroelastic domain walls in  $\text{CaTiO}_3$  are unlikely to have considerably more negative  $\Delta_{\text{seg}}E_v$ , given that the structural perturbation at domain walls is rather weak in nature, i.e., there are only gentle modifications of the octahedral tilt angles. Substantially stronger effects for other ferroelastic domains walls in  $\text{CaTiO}_3$  are consequently not to be expected.

The results of Fig. 3—oxygen-vacancy enrichment in the wall—do not translate automatically into enhanced oxygen transport rates because  $D_v^{\text{dw}}$  needs, at the very worst, to be unaffected. With the aim of obtaining this quantity, we performed MD simulations of oxygen-deficient  $\text{CaTiO}_3$  (oxygen vacancies present at a site fraction of 0.8%, and charge compensation achieved by a slight reduction in the charge of all Ti ions). The supercell contained two antiparallel domain walls and had dimensions of  $40 \times 14 \times 14$  unit cells. Unfortunately, these simulations yielded no reliable results because, at the high temperatures necessary for oxygen vacancies to execute long-range diffusion, the (antiparallel) domain walls migrated through the cell, annihilating when they met each other. (In some simulations, the unseeded creation of two antiparallel walls was also observed.) Consequently, it was not possible to isolate the effects of the domain walls on the migration of oxygen vacancies from the trapping effect of the domain walls (see Fig. 2). We were forced, therefore, to perform MS calculations. Specifically, we determined the individual barriers for oxygen-vacancy migration in and around the domain wall through nudged-elastic-band (NEB) calculations. In Fig. 4 we compare the results obtained for the regular lattice with those obtained for the domain wall.

The orthorhombic ( $Pbnm$ ) lattice of  $\text{CaTiO}_3$  is characterized, essentially, by five different activation barriers for oxygen-vacancy migration, four of which lie between 0.54 and 0.63 eV, with the fifth at 0.73 eV. Since the O1 and O2 sites differ slightly in energy, there is a small difference in activation barriers for forward and backward jumps, but because the difference is only 0.01 eV, this asymmetry is ignored for the regular lattice. The effective activation enthalpy of (long-range) oxygen-vacancy diffusion, obtained from MD simulations [17] with these potentials, is  $\Delta_{\text{mig}}H_v^{\text{eff}} = (0.58 \pm 0.02)$  eV, a result consistent with the four low-energy barriers providing continuous diffusion paths through the lattice [Fig. 4(a)]. In the domain wall, the symmetry lowering multiplies the number of different barriers. In addition, the strong variation in site energy (see Fig. 2) amplifies the asymmetry

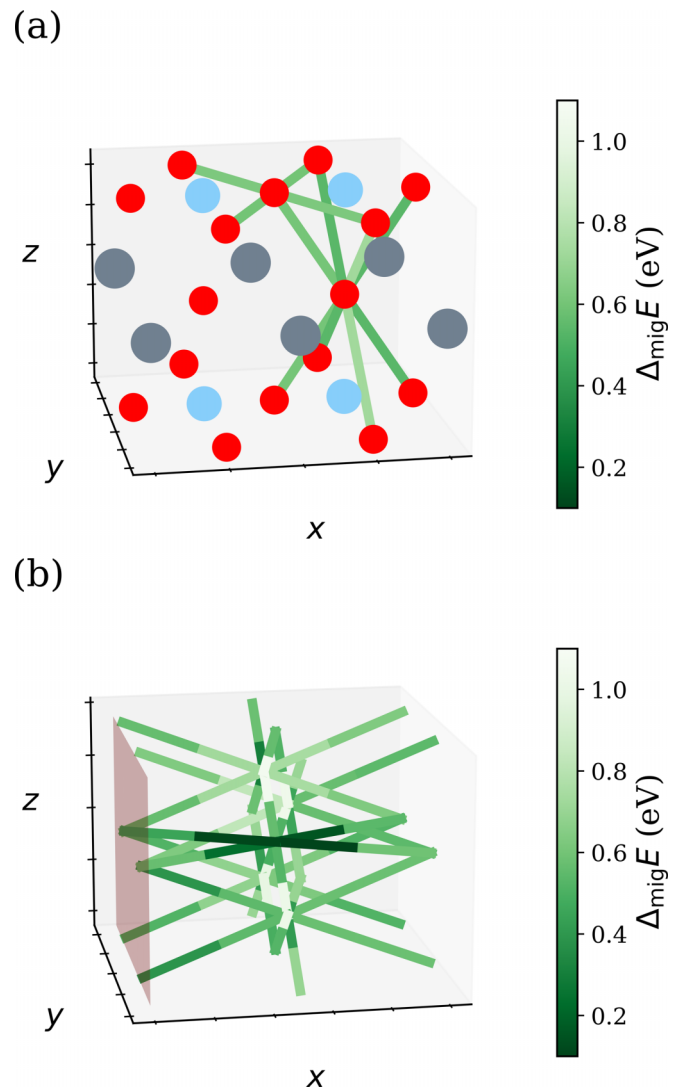


FIG. 4. Activation barriers of oxygen-vacancy migration in orthorhombic  $\text{CaTiO}_3$  obtained by NEB calculations: (a) regular lattice, with O (red), Ca (gray), Ti (blue) ions; (b) in the vicinity of the domain wall, shown as a thin plane (ions removed for clarity). Two-color paths in (b) reflect the large difference between forward and backward jumps.

between forward and backward jumps. Individual barriers now range from 0.1 to 1.1 eV, with most between 0.5 and 0.7 eV [Fig. 4(b)]. Importantly, the lowest as well as the highest barriers are isolated, so that the long-range diffusion paths will be characterized by barriers between 0.5 and 0.7 eV. Such values are not considerably lower than those in the regular lattice, and hence  $D_v^{\text{dw}}/D_v^{\text{latt}}$  will not deviate from unity by orders of magnitude, i.e., there is neither strong enhancement nor strong hindrance of oxygen-vacancy diffusion along this domain wall. This is a surprising result from two opposite points of view. The strained nature of the interface is thought [9,10] to lead to accelerated diffusion. On the other hand, the symmetry lowering within the domain wall may be expected to be detrimental, as lower symmetry in the regular lattice of  $\text{CaTiO}_3$  decreases the rate of oxygen-vacancy diffusion [17].

Taking  $\langle c_v^{\text{dw}} \rangle$  and  $D_v^{\text{dw}}$  together, we conclude that at the typical temperatures of diffusion experiments (e.g.,  $T = 1000$  K) the increase in  $D_O^{\text{dw}} [\propto \langle c_v^{\text{dw}} \rangle D_v^{\text{dw}}]$  relative to  $D_O^{\text{latt}}$  will be roughly one order of magnitude and arise predominantly from the increase in  $\langle c_v^{\text{dw}} \rangle$ . The increase of  $10^7$  reported previously [7] seems highly unlikely to correspond to domain-wall diffusion of oxygen, especially in view of  $\Delta H_{D^{\text{latt}}} \approx \Delta H_{D^{\text{dw}}} (\approx 4 \text{ eV})$  [7], and in view of doubts [17] regarding the interpretation of the measured diffusion profiles. Experimental reexamination of the issue is therefore warranted. Obtaining reliable data for  $D_O^{\text{dw}}$  may prove challenging, however, since the depletion space-charge zones will prevent oxygen from leaking away from the domain wall, and thus the (small) amount of tracer within the wall may be beyond experimental detection limits [36]. Local conductivity measurements may be more suitable, but the possibility of electronic conduction needs to be ruled out unambiguously, and in this respect obtaining an activation enthalpy of 0.4–1 eV is insufficient.

Our prediction regarding  $D_O^{\text{dw}}$  relies strongly on the twin assumptions of oxygen vacancies always being mobile and cation defects being completely immobile. The first assumption is reasonable because oxygen vacancies are mobile in perovskites even at room temperature [18], and the second is reasonable because cation vacancies are only mobile at very high temperatures [50]. For the standard case of a  $\text{CaTiO}_3$  specimen cooled continually and not too slowly from the cubic to the orthorhombic phase, both assumptions will therefore be valid. If, however, the specimen is annealed for a sufficiently long time at a temperature high enough for cations

to move but low enough for the domains to form, acceptor-type cation defects will accumulate in the space-charge zones (and may, in addition, segregate to the domain wall itself), leading ultimately to a change in  $\langle c_v^{\text{dw}} \rangle$ . Owing to the increased concentrations of cation defects, the energy landscape for oxygen-vacancy migration will be modified substantially, with an expected trend towards higher migration barriers and thus lower  $D_v$  [17,54,55]. Acceptor-type cation defects are thus unlikely to modify our conclusion drastically.

Summing up, we found that the oxygen-vacancy segregation energy at a ferroelastic domain wall behaves as a secondary order parameter in terms of Landau theory, and we used this finding, in a natural and self-consistent approach, to calculate equilibrium concentrations of oxygen vacancies within, and in the vicinity of, the wall at different temperatures. In addition, we found no large changes in  $D_v^{\text{dw}}$  relative to  $D_v^{\text{latt}}$ . We contend that these results will apply to other ferroelastic domain walls in  $\text{CaTiO}_3$  because the degree of structural perturbation will remain relatively weak. Whether the results also apply to charged domain walls in ferroelectric  $\text{BaTiO}_3$  or multiferroic  $\text{BiFeO}_3$  remains to be seen.

#### ACKNOWLEDGMENTS

Funding from the German Research Foundation (DFG) within the framework of the collaborative research center SFB 917 (Nanoswitches) is acknowledged. Simulations were performed with computing resources granted by RWTH Aachen University under Projects thes0847 and rwth0655.

- 
- [1] B. J. Kennedy, C. J. Howard, and B. C. Chakoumakos, Phase transitions in perovskite at elevated temperatures — A powder neutron diffraction study, *J. Phys.: Condens. Matter* **11**, 1479 (1999).
- [2] Y. Gu, K. Rabe, E. Bousquet, V. Gopalan, and L.-Q. Chen, Phenomenological thermodynamic potential for  $\text{CaTiO}_3$  single crystals, *Phys. Rev. B* **85**, 064117 (2012).
- [3] M. Calleja, M. T. Dove, and E. K. H. Salje, Trapping of oxygen vacancies on twin walls of  $\text{CaTiO}_3$ : A computer simulation study, *J. Phys.: Condens. Matter* **15**, 2301 (2003).
- [4] E. K. H. Salje, Ferroelastic materials, *Annu. Rev. Mater. Res.* **42**, 265 (2012).
- [5] G. Catalan, J. Seidel, R. Ramesh, and J. F. Scott, Domain wall nanoelectronics, *Rev. Mod. Phys.* **84**, 119 (2012).
- [6] D. M. Evans, V. Garcia, D. Meier, and M. Bibes, Domains and domain walls in multiferroics, *Phys. Sci. Rev.* **5**, 20190067 (2020).
- [7] I. Sakaguchi and H. Haneda, Oxygen tracer diffusion in single-crystal  $\text{CaTiO}_3$ , *J. Solid State Chem.* **124**, 195 (1996).
- [8] A. Aird and E. K. H. Salje, Enhanced reactivity of domain walls in with sodium, *Eur. Phys. J. B* **15**, 205 (2000).
- [9] W. T. Lee, E. K. H. Salje, and U. Bismayer, Ionic transport in twin domain walls, *Ferroelectrics* **303**, 3 (2004).
- [10] E. K. H. Salje, S. A. Hayward, and W. T. Lee, Ferroelastic phase transitions: Structure and microstructure, *Acta Cryst. A* **61**, 3 (2005).
- [11] L. Goncalves-Ferreira, S. A. T. Redfern, E. Artacho, E. Salje, and W. T. Lee, Trapping of oxygen vacancies in the twin walls of perovskite, *Phys. Rev. B* **81**, 024109 (2010).
- [12] U. Balachandran, B. Odekirk, and N. G. Eror, Defect structure of acceptor-doped calcium titanate at elevated temperatures, *J. Mater. Sci.* **17**, 1656 (1982).
- [13] U. Balachandran, B. Odekirk, and N. Eror, Electrical conductivity in calcium titanate, *J. Solid State Chem.* **41**, 185 (1982).
- [14] T. Bak, J. Nowotny, C. C. Sorrell, and M. F. Zhou, Electronic and ionic conductivity in  $\text{CaTiO}_3$ , *Ionics* **10**, 334 (2004).
- [15] K. Wright and G. D. Price, Computer simulation of defects and diffusion in perovskites, *J. Geophys. Res.: Solid Earth* **98**, 22245 (1993).
- [16] G. C. Mather, M. S. Islam, and F. M. Figueiredo, Atomistic study of a  $\text{CaTiO}_3$ -based mixed conductor: Defects, nanoscale clusters, and oxide-ion migration, *Adv. Funct. Mater.* **17**, 905 (2007).
- [17] E. Robens, R. Rauschen, J. Kaub, J. P. Parras, D. Kemp, C. L. Freeman, and R. A. De Souza, Perovskite crystal symmetry and oxygen-ion transport: a molecular-dynamics study of perovskite, *J. Mater. Chem. A* **10**, 2388 (2022).
- [18] R. A. De Souza, Oxygen diffusion in  $\text{SrTiO}_3$  and related perovskite oxides, *Adv. Funct. Mater.* **25**, 6326 (2015).
- [19] J. D. Gale, GULP: A computer program for the symmetry-adapted simulation of solids, *J. Chem. Soc. Faraday Trans.* **93**, 629 (1997).
- [20] S. Plimpton, Fast parallel algorithms for short-range molecular dynamics, *J. Comput. Phys.* **117**, 1 (1995).

- [21] A. Pedone, G. Malavasi, M. C. Menziani, A. N. Cormack, and U. Segre, A new self-consistent empirical interatomic potential model for oxides, silicates, and silicas-based glasses, *J. Phys. Chem. B* **110**, 11780 (2006).
- [22] L. Goncalves-Ferreira, S. A. T. Redfern, E. Artacho, and E. K. H. Salje, Ferrielectric Twin Walls in  $\text{CaTiO}_3$ , *Phys. Rev. Lett.* **101**, 097602 (2008).
- [23] R. Rauschen, octa-tilt-perov: First light (2021), <https://github.com/robertrauschen/octa-tilt-perov/>
- [24] W. T. Lee, E. K. H. Salje, L. Goncalves-Ferreira, M. Daraktchiev, and U. Bismayer, Intrinsic activation energy for twin-wall motion in the ferroelastic perovskite  $\text{CaTiO}_3$ , *Phys. Rev. B* **73**, 214110 (2006).
- [25] A. H. H. Ramadan and R. A. De Souza, Atomistic simulations of symmetrical low-angle [100] (011) tilt boundaries in  $\text{SrTiO}_3$ , *Acta Mater.* **118**, 286 (2016).
- [26] N. F. Mott and M. J. Littleton, Conduction in polar crystals. I. Electrolytic conduction in solid salts, *Trans. Faraday Soc.* **34**, 485 (1938).
- [27] P. C. McIntyre, Equilibrium point defect and electronic carrier distributions near interfaces in acceptor-doped strontium titanate, *J. Am. Ceram. Soc.* **83**, 1129 (2000).
- [28] R. A. De Souza, The formation of equilibrium space-charge zones at grain boundaries in the perovskite oxide  $\text{SrTiO}_3$ , *Phys. Chem. Chem. Phys.* **11**, 9939 (2009).
- [29] H.-S. Lee, T. Mizoguchi, J. Mitsui, T. Yamamoto, S.-J. L. Kang, and Y. Ikuhara, Defect energetics in  $\text{SrTiO}_3$  symmetric tilt grain boundaries, *Phys. Rev. B* **83**, 104110 (2011).
- [30] M. Behtash, Y. Wang, J. Luo, and K. Yang, Oxygen vacancy formation in the  $\text{SrTiO}_3 \Sigma 5$  [001] twist grain boundary from first-principles, *J. Am. Ceram. Soc.* **101**, 3118 (2018).
- [31] C. Tao, D. Mutter, D. F. Urban, and C. Elsässer, Atomistic calculations of charged point defects at grain boundaries in  $\text{SrTiO}_3$ , *Phys. Rev. B* **104**, 054114 (2021).
- [32] R. A. De Souza and M. Martin, Using  $^{18}\text{O}/^{16}\text{O}$  exchange to probe an equilibrium space-charge layer at the surface of a crystalline oxide: method and application, *Phys. Chem. Chem. Phys.* **10**, 2356 (2008).
- [33] R. A. De Souza, V. Metlenko, D. Park, and T. E. Weirich, Behavior of oxygen vacancies in single-crystal  $\text{SrTiO}_3$ : Equilibrium distribution and diffusion kinetics, *Phys. Rev. B* **85**, 174109 (2012).
- [34] J. Carrasco, F. Illas, N. Lopez, E. A. Kotomin, Y. F. Zhukovskii, R. A. Evarestov, Y. A. Mastrikov, S. Piskunov, and J. Maier, First-principles calculations of the atomic and electronic structure of  $F$  centers in the bulk and on the (001) surface of  $\text{SrTiO}_3$ , *Phys. Rev. B* **73**, 064106 (2006).
- [35] Y.-L. Lee and D. Morgan, *Ab initio* defect energetics of perovskite (001) surfaces for solid oxide fuel cells: A comparative study of  $\text{LaMnO}_3$  versus  $\text{SrTiO}_3$  and  $\text{LaAlO}_3$ , *Phys. Rev. B* **91**, 195430 (2015).
- [36] V. Metlenko, A. H. H. Ramadan, F. Gunkel, H. Du, H. Schraknepper, S. Hoffmann-Eifert, R. Dittmann, R. Waser, and R. A. De Souza, Do dislocations act as atomic autobahns for oxygen in the perovskite oxide  $\text{SrTiO}_3$ , *Nanoscale* **6**, 12864 (2014).
- [37] D. Marrocchelli, L. Sun, and B. Yildiz, Dislocations in  $\text{SrTiO}_3$ : Easy to reduce but not so fast for oxygen transport, *J. Am. Chem. Soc.* **137**, 4735 (2015).
- [38] S. P. Waldow and R. A. De Souza, Computational study of oxygen diffusion along  $a$ [100] dislocations in the perovskite oxide  $\text{SrTiO}_3$ , *ACS Appl. Mater. Interfaces* **8**, 12246 (2016).
- [39] R. A. De Souza and E. C. Dickey, The effect of space-charge formation on the grain-boundary energy of an ionic solid, *Philos. Trans. R. Soc. A* **377**, 20180430 (2019).
- [40] N. H. Chan, R. K. Sharma, and D. M. Smyth, Nonstoichiometry in  $\text{SrTiO}_3$ , *J. Electrochem. Soc.* **128**, 1762 (1981).
- [41] R. Moos and K. H. Härdtl, Defect chemistry of donor-doped and undoped strontium titanate ceramics between 1000° and 1400°C, *J. Am. Ceram. Soc.* **80**, 2549 (2005).
- [42] M. Siebenhofer, F. Baiutti, J. de Dios Sirvent, T. M. Huber, A. Viernstein, S. Smetaczek, C. Herzig, M. O. Liedke, M. Butterling, A. Wagner, E. Hirschmann, A. Limbeck, A. Tarancon, J. Fleig, and M. Kubicek, Exploring point defects and trap states in undoped  $\text{SrTiO}_3$  single crystals, *J. Eur. Ceram. Soc.* **42**, 1510 (2022).
- [43] N.-H. Chan, R. Sharma, and D. M. Smyth, Nonstoichiometry in undoped  $\text{BaTiO}_3$ , *J. Am. Ceram. Soc.* **64**, 556 (1981).
- [44] P. Erhart and K. Albe, Modeling the electrical conductivity in  $\text{BaTiO}_3$  on the basis of first-principles calculations, *J. Appl. Phys.* **104**, 044315 (2008).
- [45] M. Kessel, R. A. De Souza, and M. Martin, Oxygen diffusion in single crystal barium titanate, *Phys. Chem. Chem. Phys.* **17**, 12587 (2015).
- [46] K. S. Belthle, U. N. Gries, M. P. Mueller, D. Kemp, A. Prakash, M.-A. Rose, J. M. Börgers, B. Jalan, F. Gunkel, and R. A. De Souza, Quantitative determination of native point-defect concentrations at the ppm level in un-doped  $\text{BaSnO}_3$  thin films, *Adv. Funct. Mater.* **32**, 2113023 (2022).
- [47] J. Jamnik, J. Maier, and S. Pejovnik, Interfaces in solid ionic conductors: Equilibrium and small signal picture, *Solid State Ionics* **75**, 51 (1995).
- [48] J. H. Barrett, Dielectric constant in perovskite type crystals, *Phys. Rev.* **86**, 118 (1952).
- [49] V. V. Lemanov, A. V. Sotnikov, E. P. Smirnova, M. Weihnacht, and R. Kunze, Perovskite  $\text{CaTiO}_3$  as an incipient ferroelectric, *Solid State Commun.* **110**, 611 (1999).
- [50] R. A. De Souza, Ion transport in metal oxides, in *Resistive Switching* (Wiley-VCH, Weinheim, 2016), pp. 125–164.
- [51] Y. Zuo, Y. A. Genenko, A. Klein, P. Stein, and B. Xu, Domain wall stability in ferroelectrics with space charges, *J. Appl. Phys.* **115**, 084110 (2014).
- [52] Y. Zuo, Y. A. Genenko, and B.-X. Xu, Charge compensation of head-to-head and tail-to-tail domain walls in barium titanate and its influence on conductivity, *J. Appl. Phys.* **116**, 044109 (2014).
- [53] E. A. Eliseev, A. N. Morozovska, Y. Gu, A. Y. Borisevich, L. Q. Chen, V. Gopalan, and S. V. Kalinin, Conductivity of twin-domain-wall/surface junctions in ferroelastics: Interplay of deformation potential, octahedral rotations, improper ferroelectricity, and flexoelectric coupling, *Phys. Rev. B* **86**, 085416 (2012).
- [54] M. Schie, R. Waser, and R. A. De Souza, A simulation study of oxygen-vacancy behavior in strontium titanate: Beyond nearest-neighbor interactions, *J. Phys. Chem. C* **118**, 15185 (2014).
- [55] H. Zhang and R. A. De Souza, Optimising oxygen diffusion in non-cubic, non-dilute perovskite oxides based on  $\text{BiFeO}_3$ , *J. Mater. Chem. A* **7**, 25274 (2019).